

Morphology of evening sector aurorae in $\lambda 557.7$ -nm Doppler temperatures

J. M. Holmes¹, M. Conde², C. Deehr, and D. Lummerzheim

Geophysical Institute, University of Alaska Fairbanks

An all-sky scanning Fabry-Pérot spectrometer was used to observe temperatures of auroral OI(557.7-nm) emissions over Poker Flat. The sudden temporal and spatial changes in Doppler temperatures that were observed are likely due to the emission height changing as a response to variations in the characteristic energy of the precipitating electron population. Three cases were analyzed: (1) A Doppler temperature drop (~ 200 K) over the entire sky occurred immediately after an auroral brightening; the temperature remained lower after the auroral intensity had resumed its quiescent levels. (2) A local increase of Doppler temperature, colocated with a weak auroral arc, occurred 25 minutes before a westward propagating substorm onset. When the auroral luminosity suddenly increased the Doppler temperature had a sharp decrease. (3) The region inside a loop like auroral arc showed elevated Doppler temperature relative to that of the arc itself. Auroral fading just prior to onset was accompanied by increased temperatures.

1. Introduction

Beginning with the original interferometric measurements of the auroral $\lambda 557.7$ -nm line by Babcock [1923], there has been considerable interest in the measurement of auroral and airglow emissions and their applications to upper atmospheric physics. Determination of temperatures from Doppler-broadened emissions, including both atomic [Armstrong, 1958; Wark, 1959; Nilson and Shepherd, 1960] and molecular species [Vegard, 1932; Lytle and Hunten, 1960], contributed to the early quantification of thermospheric and mesospheric temperatures. A discussion of the applications of optical Doppler measurements for this era is given by Hunten [1961].

More recently, interferometric techniques have been used with an emphasis on determining neutral winds from observed Doppler shifts [Hernandez and Killeen, 1988]. Investigations of thermospheric dynamics have been made using these techniques ranging from small-scale studies of specific phenomena [Rees, 1984b] to global-scale observations [Killeen *et al.*, 1988].

With the advent of the ground-based all-sky Fabry-Pérot spectrometer (ASI-FPS) [Rees and Greenaway, 1983; Rees *et al.*, 1984a; Biondi *et al.*, 1995; Nakajima *et al.*, 1995; Ishii *et al.*, 1997; Conde and Smith, 1995, 1997], it became possible to record Doppler spectra in many locations across the sky, as opposed to previous narrow-field Fabry-Pérot spectrometers which routinely observed only the zenith plus the four cardinal azimuths. This novel technique that provides modest spatial resolution is now used to explore the relationship between auroral intensity and Doppler temperature.

The auroral $\lambda 557.7$ -nm [O I] emission is a result of the metastable transition between the excited ¹D and ¹S states of atomic oxygen, the bulk of which is produced in the height range of 100-150 km. The state has a lifetime of 0.74s, which provides adequate time for thermalization in this altitude range. Thus, it can be tacitly assumed that the emitting population is in thermal equilibrium with the neutral atmosphere. Since the thermosphere has a positive temperature gradient, higher energy electron precipitation, which penetrates farther into the lower thermosphere, produces more intense aurora with lower temperatures as measured by all-sky instruments such as the Scanning Doppler Imager [Rees, 1989].

This inverse relationship between Doppler temperature and auroral intensity has long been known [Størmer, 1955], and is known to persist in spite of increased localized Joule heating [Ishii *et al.*, 2001]. Narrow-field interferometric measurements of auroral Doppler temperatures, when compared with intensities, show an identical relationship, although deviations from simple inverse-proportionality are observed [Hilliard and Shepherd, 1966]. Owing to the known relations between observed temperatures and intensities, optical temperature data, in the absence of auxiliary height information, are of limited use in estimating the rate of auroral energy deposition and Joule heating [Turgeon and Shepherd, 1962].

2. Instrumentation

The Poker Flat SDI makes measurements of the $\lambda 557.7$ -nm [O I] emission using an imaging Fabry-Pérot capacitance-stabilized étalon of 20-mm air-spaced gap and 105-mm working aperture. The all-sky optics of the instrument have a 140° field of view. The imager is unique in that unlike other imaging FPS instruments, the SDI acquires spectra by repeatedly scanning the Fabry-Pérot étalon plate separation through one order of interference, producing spectra as a function of étalon gap (as opposed

¹Now at the University Centre in Svalbard, Longyearbyen, Norway

²Now at Latrobe University, Melbourne, Australia

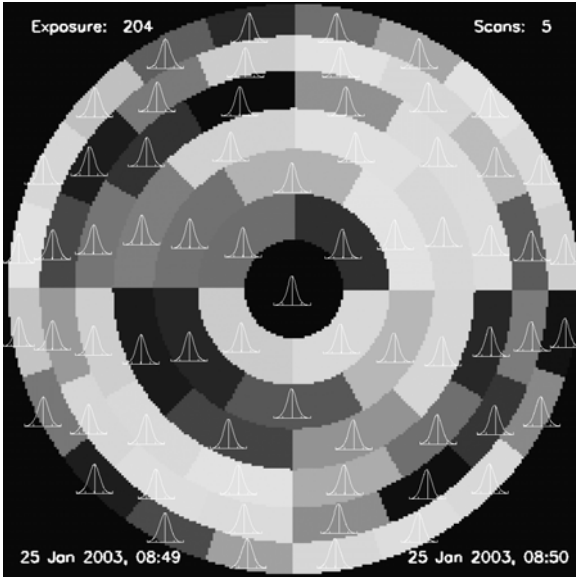


Figure 1. Example SDI $\lambda 557.7$ -nm zone map with fitted spectra (white). Exposure time: 1 minute. Background shading depicts zone boundaries.

to the individual fringe shape) [Conde *et al.*, 2001a]. This allows the acquisition of images and spectra which are not distorted by temporal and spatial brightness fluctuations in the aurora during one scan [Conde and Smith, 1997].

To produce high signal-to-noise spectra with integration times on the order of minutes, the SDI analysis software divides images into arbitrary “zones”, the overall signal in each zone yielding an individual spectrum. Figure 1 shows the zones and their recorded spectra for a one-minute integration. By fitting each spectrum with a suitable model profile (in this case, a Gaussian emission function convolved with a measured instrument function), the Doppler broadening, Doppler shift and emission and background brightnesses are determined. Doppler shifts provide line-of-sight winds, while Doppler broadening, when calibrated, returns the temperature of the emitting population.

For the cases analyzed, the SDI is configured to group signal into 67 zones, thereby providing modest spatial resolution without resorting to longer integration times unsuitable to investigate the desired temporal auroral structure. In order to ensure consistent uncertainties and signal levels, the integration time is automatically adjusted during observations according to signal brightness, with exposure times varying from about 1 minute for bright and 7-8 minutes for very weak aurora.

Uncertainties in calculated temperatures vary depending on auroral intensities and also the location of the zone relative to the zenith, but are typically between 5 and 10 degrees Kelvin under bright auroral conditions. Figure 2(a, b, c) are histograms of temperature uncertainty and their variation with zone number (zone numbers increase with zenith angle). Also, Figure 2(d) shows the decrease of temperature uncertainty with auroral intensity. A description of the treatment and determination of uncertainties can be found in Conde [2001b]; a detailed

discussion of instrumental particulars can be found in Conde and Smith [1995].

3. Observations

Three cases were chosen to illustrate different types of dynamics of the $\lambda 557.7$ -nm optical temperature relative to the motions of the visible aurora. All cases display evening sector discrete aurora and/or substorm activity. Although measurement of temperature derived from the spectral width of auroral emissions can be used in part for identifying Joule and particle heating, care must be taken since it is well known that the height of emission (and therefore the temperature in the ideal thermosphere) varies primarily by changes in the energy spectrum of the particle precipitation [Sica *et al.*, 1996].

3.1 Case 1: December 2, 2002

The first case was observed on December 2, 2002. Figure 3 shows the SDI data in an image sequence of temperature maps. For reference, the Geophysical Institute white light all-sky camera is shown above the maps.

Since the previous brightening event at 0844 UT (not shown), a gradual increase in measured temperature occurred, starting near zenith then nearly filling the entire field of view of the instrument at about 0930 UT. This is depicted in the first two images in Figure 3, at 0944 and 0947 UT. It is interesting to note that there was little or no change in the measured brightness during this period of “warming”.

The westward-propagating brightening event at 0949 UT displays an immediate temperature drop of roughly 200K within the intensified region. Note that after the intensity enhancement had passed (either dimming overhead or advecting out of the instrument’s field of view), the lower temperature present during the event persisted for many tens of minutes thereafter.

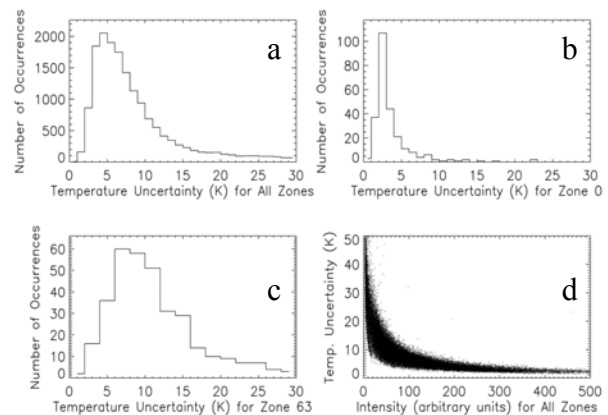


Figure 2. Temperature uncertainty histograms calculated for 22 March 2003: all zones (a), zenith zone (b), edge zone (c). A scatter plot showing temperature uncertainty versus intensity is shown in (d).

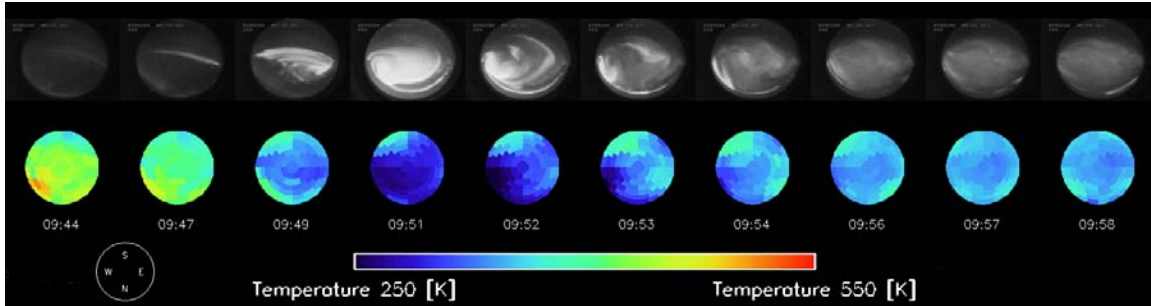


Figure 3. An image sequence depicting an auroral brightening event and associated changes in the $\lambda 557.7$ -nm optical temperature for 2 December 2002 from 0944 to 0958 UT. The upper row shows the Poker Flat All-sky Camera and the lower row shows the temperature maps produced by the Scanning Doppler Imager

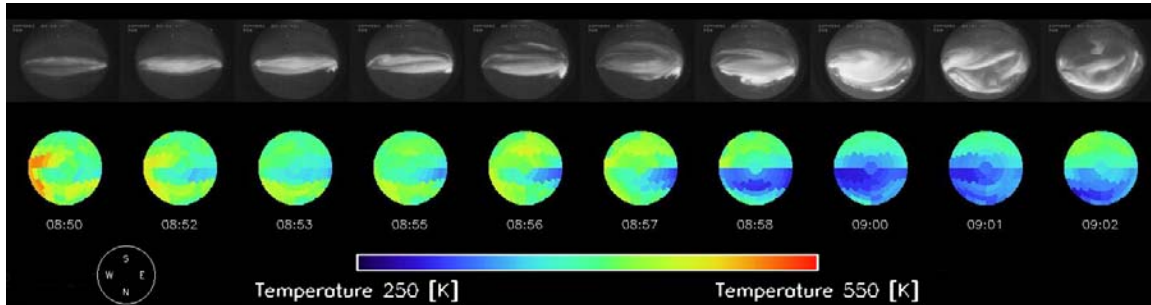


Figure 4. A time series depicting an auroral brightening event and associated changes in the $\lambda 557.7$ -nm optical temperature for 22 March 2003 from 0850 to 0909 UT.

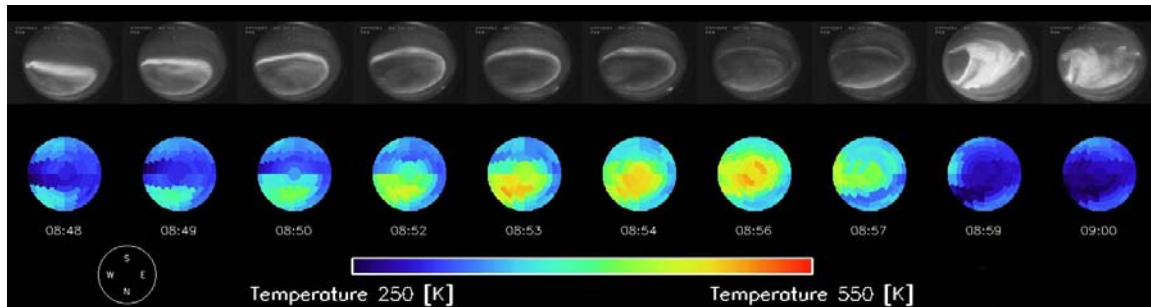


Figure 5. A time series showing the WTS event on 24 March 2003 from 0848 to 0900 UT. Note that as the loop-like feature moves westward, the region of elevated optical temperature inside it appears to follow the movement.

3.2 Case 2: March 22, 2003

The second case was observed on March 22, 2002. The sequence in Figure 4 shows a band of discrete arcs near zenith accompanied by a relatively high temperature (shown in yellow and red). Preceding the beginning of the sequence, a thin arc of both increasing temperature and brightness was observed slightly equatorward of the brightening arc shown in the first frame in the figure. Immediately after the emission intensity began to increase at approximately 0852 UT, a temperature drop occurred only in the vicinity of the brightening features, i.e. from zenith eastward toward the edge of the temperature map (0856 – 0858 UT). This case illustrates large gradients and discrete features in the temperature data evolving in only several minutes.

3.3 Case 3: March 24, 2003

The final and most interesting case occurred on March 24, 2002. Figure 5 shows the time evolution of a westward-traveling arc. The SDI measured low to moderate temperatures in the vicinity of the discrete loop-like band, which is expected based on previous measurements. However, inside the band, a much warmer region developed (0852-0857 UT) shortly before the band broke up at 0859 UT, filling almost the entire field of view with aurora.

Figure 6 depicts the elevation of neutral temperature in the zenith zone during the above time period. The ratio of the $\lambda 630.0$ -nm [O I] emission to the $\lambda 427.8$ -nm (N_2^+) emission, as measured by the Meridian Scanning Photometer (MSP) at Poker Flat, was used to make an estimate of the characteristic energy of deposited auroral electrons in the magnetic zenith using a technique

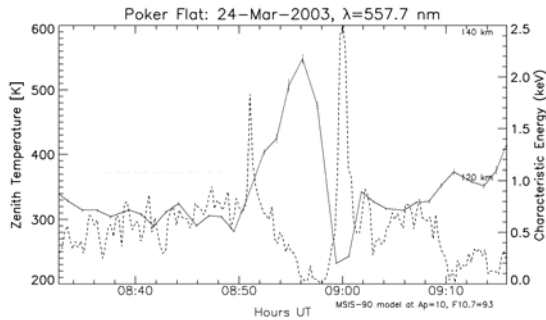


Figure 6. Time series of zenith temperature (solid line) and derived characteristic energy (dashed line) between 0832 and 0916 UT on 24 March, 2003. Dotted lines represent MSIS-90 heights.

described in *Lummerzheim, et al.* [1990]. The figure indicates a decreased characteristic energy, which follows if it is assumed that the increase in Doppler temperature resulted, at least partly, from an increase in the emission altitude.

4. Discussion

There exist commonalities between all three cases discussed in this study. First, when considering discrete arcs, the combined SDI and ASC data clearly show the commonly accepted inverse relationship between auroral intensity and temperature.

Next, as mentioned earlier, the data frequently exhibit large temperature variations over very short spatial and temporal scales. Several median temperature time series, taken over the entire field of view, have shown changes in temperature of hundreds of degrees Kelvin in a matter of only several minutes. For the first case of December 2, 2002, shortly after 0800 UT (not shown), a near all-sky brightening event occurred and the measured temperature from the SDI dropped nearly 200K. Since the temperature decreased, it is evident that auroral heating or possibly other *in situ* thermospheric dynamics are not primarily responsible for the bulk of the temperature change; the drop occurred from a sudden lowering of the altitude of auroral energy deposition, which corresponds to an increase in characteristic energy. However, neutral heating is almost certainly taking place, since it draws more than 50% of the power associated with auroral particle precipitation [*Rees et al.*, 1983]. The presence of heating in the emitting region causes the estimated emission height to be overestimated (when simply converting from temperature using a model such as MSIS); the actual height of emission could in fact be lower depending on the amount of heating.

It is also noteworthy that for the case of 0848-0900UT on 24 March 2003, the portion of the loop-like feature closest to the zenith decreased in intensity from 15 kR at 0854 UT to 3 kR immediately before the onset westward-traveling surge. The $\lambda 427.8$ -nm channel of the MSP revealed a similar reduction while the $\lambda 630.0$ -nm channel remained approximately constant. This sudden increase in

the red/blue ratio and corresponding decrease in characteristic energy is indicative of “auroral fading” as described by *Pellinen and Heikkila* [1978]. Although the softening of the auroral precipitation was not accompanied by a significant increase in number flux, and the equatorward hydrogen arc detected by the MSP $\lambda 486.1$ -nm ($H\beta$) channel did not move significantly during this “fading” period, the region of enhanced $\lambda 557.7$ -nm Doppler temperature, located just equatorward of this arc, increased in temperature by at least 100K in only several minutes prior to surge onset.

5. Conclusions

The case studies presented here are only interpreted qualitatively; they are used to illustrate some of the phenomenology of the neutral thermosphere Doppler temperature in the auroral energy deposition region and its relation to optical auroral emissions. In addition, the Doppler temperatures recorded using this imaging instrument show variations with respect to auroral activity that are consistent with older non-imaging instruments. Although temperature data from the Scanning Doppler Imager alone cannot be used to deduce the sources of the dynamics observed, it is nonetheless an indispensable instrument for the observation of spatially resolved phenomena in the vicinity of auroral arcs and the characterization of neutral atmospheric properties in the context of auroral effects on the thermosphere.

Acknowledgments. This work was supported by a joint NASA and NSF TIMED-CEDAR grant, number NAG5-10069. We would also like to thank Brian Lawson for the operation of the Poker Flat All-sky Camera and Meridian Scanning Photometer.

References

- Armstrong, E. B. The temperature in the atmospheric region emitting the nightglow OI 5577 line and in regions above faint auroral arcs, *J. Atmos. Terr. Phys.*, *13*, 205-216, 1959.
- Biondi, M. A., D. P. Sipler, M. E. Zipf, and J. L. Baumgardner, All-sky Doppler interferometer for thermospheric dynamics studies, *Appl. Opt.*, *34*, 1646-1654, 1995.
- Conde, M. and R. Smith. Mapping thermospheric winds in the auroral zone, *Geophys. Res. Lett.*, *22*, 3019-3022, 1995.
- Conde, M. and R. Smith. Phase compensation of a separation scanned, all-sky imaging Fabry-Pérot spectrometer for auroral studies, *Appl. Opt.*, *36*, 5441-5450, 1997.
- Conde, M., J. D. Craven, T. Immel, E. Hoch, H. Stenbaek-Nielsen, T. Hallinan, R. W. Smith, J. Olson, and Wei Sun, Assimilated observations of thermospheric winds, the aurora, and ionospheric currents over Alaska, *J. Geophys. Res.*, *106*, 10493-10508, 2001.
- Conde, M, Analysis of Fabry-Pérot spectra of lidar backscatter echoes, *ANARE Reports*, edited by Morris, R. J. et al., 146, 91-114, 2001.
- Hernandez, G. and T. L. Kilean, Optical measurements of winds and kinetic temperatures in the upper atmosphere, *Adv. Space. Res.*, *8*(5), 149-213, 1988.
- Hilliard, R., L. and G. G. Shepherd, Upper atmospheric temperatures from Doppler line widths -IV, A detailed study using the OI 5577 Å auroral and nightglow emission, *Planet. Space Sci.*, *14*, 383-406.
- Hunten, D. M., Temperatures deduced from aurora and airglow spectra, *Ann. Géophys.*, *17*, 249, 1961.

- Ishii, M., M. Conde, R. W. Smith, M. Krynicki, E. Sagawa, and S. Watari, Vertical wind observations with two Fabry-Pérot interferometers at Poker Flat, Alaska, *J. Geophys. Res.*, **106**, 10537-10551, 2001.
- Ishii, M., S. Okano, E. Sagawa, S. Watari, H. Mori, I. Iwamoto, and Y. Myrayama, Development of Fabry-Pérot interferometers for airglow observations, *Proc. NIPR Symp. Upper Atmos. Phys.*, **10**, 97-108, 1997.
- Killeen, T. L., J. D. Craven, L. A. Frank, J. J. Ponthieu, N. W. Spencer, R. A. Heelis, L. H. Brace, R. G. Roble, P. B. Hays, and G. R. Carnigan, On the relationship between dynamics of the polar thermosphere and morphology of the aurora: Global-scale observations from Dynamics Explorers 1 and 2, *J. Geophys. Res.*, **93**, 2675-2692, 1988.
- Lummerzheim, D., M. H. Rees, and G. J. Romick, The application of spectroscopic studies of the aurora to thermospheric neutral composition, *Planet. Space Sci.*, **38**, 67-68, 1990.
- Lummerzheim, D., and J. Lilensten, Electron transport and energy degradation in the ionosphere: evaluation of the numerical solution, comparison with laboratory experiments and auroral observations, *Ann. Geophys.*, **12**, 1039-1051, 1994.
- Lytle, E. A. and D. M. Hunten, Dawn enhancement of Auroral N_2^+ emission, *Can. J. Phys.*, **38**, 477, 1960.
- Nakajima, H., S. Okano, H. Fukunishi, and T. Ono, Observations of thermospheric wind velocities and temperatures by use of a Fabry-Pérot Doppler imaging system at Syowa Station, Antarctica, *Appl. Opt.*, **34**, 8382-8395, 1995.
- Nilson, J. A. and G. G. Shepherd, Upper atmospheric temperatures from Doppler line widths -I. Some preliminary measurements on OI 5577 Å in aurora, *Planet. Space Sci.*, **5**, 299-306, 1961.
- Pellinen, R. J., and W. J. Heikkila, Observations of auroral fading before breakup, *J. Geophys. Res.*, **83**, 4207, 1978.
- Rees, D., and A. H. Greenaway, Doppler imaging system, an optical device for measuring vector winds, I, General principles, *Appl. Opt.*, **22**, 1078-1083, 1983.
- Rees, D., A. H. Greenaway, R. Gordon, I. McWhirter, P. J. Charleton, and Å. Steen, The Doppler imaging system, initial observations of the auroral thermosphere, *Planet. Space Sci.*, **32**, 273-285, 1984a.
- Rees, D., R. W. Smith, P. J. Charleton, F. G. McCormac, N. Lloyd, and Å. Steen, The generation of vertical winds and gravity waves at auroral latitudes, I, Observations of vertical winds, *Planet. Space Sci.*, **38**, 667-684, 1984b.
- Rees, M. H., B. A. Emery, R. G. Roble, and K. Stamnes, Neutral and ion gas heating by auroral electron precipitation, *J. Geophys. Res.*, **88**, 6289-6300, 1983.
- Rees, M. H., Physics and chemistry of the upper atmosphere, Cambridge, New York, 1989.
- Størmer, C., The polar aurora, Clarendon Press, Oxford, 1955.
- Turgeon, E. C. and G. G. Shepherd, Upper atmospheric temperatures from Doppler line widths -II, Measurements on the OI 5577 and OI 6300 Å lines in aurora, *Planet. Space Sci.*, **9**, 295-304.
- Vegard, L., Results of investigations of the auroral spectrum during the years 1921-1936, *Geophys. Publ.*, **9(11)**, 1-71, 1932.
- Wark, D. Q., Doppler widths of the atomic oxygen lines in the airglow, *Astrophys. J.*, **131**, 491-501, 1960.